Mechanisms Underlying the Neuromodulation of Spinal Circuits for Correcting Gait and Balance Deficits after Spinal Cord Injury

Highlights

- Simulations reproduce motor pattern formation during epidural electrical stimulation

- Epidural electrical stimulation modulates muscle spindle feedback circuits

- Simulations lead to novel stimulation protocols correcting gait and balance deficits

- This new conceptual framework improves stimulation protocols for clinical applications

Authors

Eduardo Martin Moraud,
Marco Capogrosso,
Emanuele Formento, Nikolaus Wenger,
Jack DiGiovanna, Grégoire Courtine,
Silvestro Micera

Correspondence

gregoire.courtine@epfl.ch (G.C.),
silvestro.micera@epfl.ch (S.M.)

In Brief

Computer simulations validated experimentally revealed that epidural electrical stimulation of lumbar segments facilitates motor control through the modulation of muscle spindle feedback circuits. Simulations established a clinical framework to design stimulation protocols correcting gait symmetry and balance deficits after injury.

Mechanisms Underlying the Neuromodulation of Spinal Circuits for Correcting Gait and Balance Deficits after Spinal Cord Injury

Eduardo Martin Moraud,[1,4] Marco Capogrosso,[1,2,4] Emanuele Formento,[1] Nikolaus Wenger,[1,3] Jack DiGiovanna,[1] Grégoire Courtine,[1,5,*] and Silvestro Micera[1,2,5,*]
[1]Swiss Federal Institute of Technology (EPFL), 1015 Lausanne, Switzerland
[2]BioRobotics Institute, Scuola Superiore Sant'Anna, 56127 Pisa, Italy
[3]Department of Neurology and Experimental Neurology, University of Berlin, 10098 Berlin, Germany
[4]Co-first author
[5]Co-senior author
*Correspondence: gregoire.courtine@epfl.ch (G.C.), silvestro.micera@epfl.ch (S.M.)
http://dx.doi.org/10.1016/j.neuron.2016.01.009

SUMMARY

Epidural electrical stimulation of lumbar segments facilitates standing and walking in animal models and humans with spinal cord injury. However, the mechanisms through which this neuromodulation therapy engages spinal circuits remain enigmatic. Using computer simulations and behavioral experiments, we provide evidence that epidural electrical stimulation interacts with muscle spindle feedback circuits to modulate muscle activity during locomotion. Hypothesis-driven strategies emerging from simulations steered the design of stimulation protocols that adjust bilateral hindlimb kinematics throughout gait execution. These stimulation strategies corrected subject-specific gait and balance deficits in rats with incomplete and complete spinal cord injury. The conservation of muscle spindle feedback circuits across mammals suggests that the same mechanisms may facilitate motor control in humans. These results provide a conceptual framework to improve stimulation protocols for clinical applications.

INTRODUCTION

Severe spinal cord injury (SCI) disrupts the communication between supraspinal centers and spinal circuits producing leg movement. The interruption of descending pathways abolishes the sources of modulation and excitation that are essential to enable functional states of spinal circuits (Courtine et al., 2009; Kiehn, 2006; Orlovsky et al., 1999). Albeit intact, denervated lumbar circuits remain in a state that is not permissive for standing and walking. Electrical epidural stimulation (EES) of lumbar segments provides a strategy to reactivate these circuits (Angeli et al., 2014; Carhart et al., 2004; Hofstoetter et al., 2015). For example, individuals with a chronic, functionally complete SCI immediately regained the ability to stand and produce voluntary movements during continuous EES of lumbar segments (Angeli et al., 2014).

These preliminary results have triggered the deployment of clinical studies that evaluate the potential of EES to improve motor recovery after SCI. However, the mechanisms through which EES enables the production of motor patterns remain enigmatic, even though this understanding is pivotal in the translation of this paradigm into a viable clinical application. Computer simulations (Capogrosso et al., 2013; Rattay et al., 2000) and experimental studies (Gerasimenko et al., 2006; Hofstoetter et al., 2015) provided evidence that EES primarily engages large myelinated fibers associated with proprioceptive and cutaneous feedback circuits. The prevailing view is that the recruitment of these fibers raises the excitability of spinal circuits and modulates central pattern generator networks (Angeli et al., 2014; Danner et al., 2015). This conceptual framework has restricted the clinical application of EES to continuous, non-modulated stimulation patterns (Angeli et al., 2014; Carhart et al., 2004; Hofstoetter et al., 2015). However, this strategy fails to address subject-specific deficits of gait and balance throughout movement execution, which is essential to maximize the outcome of rehabilitation protocols (Barbeau et al., 1999; Edgerton et al., 2008).

In this study, we hypothesized that EES paradigms exploiting the dynamic properties of spinal circuits in real time provide the opportunity to target subject-specific motor deficits, mediating superior therapeutic effects compared to tonic stimulation. We previously showed that closed-loop control of EES is capable of modulating gait features during locomotion in rats with complete SCI (Wenger et al., 2014). However, the design of EES paradigms that ecologically interact with spinal circuit dynamics is contingent on a mechanistic understanding of how the recruitment of large myelinated fibers translates into modulation of muscle activity (Courtine and Bloch, 2015).

Computational models have played an important role in guiding the application of neuromodulation therapies to alleviate motor deficits in Parkinson's disease (McIntyre and Foutz, 2013) and neuropathic pain (Zhang et al., 2014). Here, we developed

a computational model that predicts the interactions between EES and spinal circuit dynamics. Simulations uncovered the mechanisms through which EES interacts with muscle spindle feedback circuits to modulate standing and walking in the absence of supraspinal contribution. We found that spinal circuits filter the modulating effects of EES toward functionally relevant pathways. This finding steered the design of stimulation protocols that reestablished gait symmetry and corrected balance deficits in rats with incomplete and complete SCI. These results establish a computational framework for the development of neuromodulation therapies that harness spinal circuit dynamics to facilitate rehabilitation and recovery in patients with SCI.

RESULTS

Dynamic Model Combining Realistic Neuronal Networks Coupled to Hindlimb Biomechanics

To study the mechanisms through which EES leads to motor pattern formation, we elaborated a dynamic model wherein muscle spindle feedback circuits receive natural sensory input from realistic hindlimb neurobiomechanics.

First, we modeled muscle spindle feedback pathways and integrated these circuits within the minimal neuronal network that is responsible for the reciprocal recruitment of agonist muscles. This neural network, inspired from experimental (Jankowska, 1992; Talpalar et al., 2011) and computational studies (Stienen et al., 2007), embeds realistic S alpha motoneurons (Figures 1D and S1A) (Booth et al., 1997; Jones and Bawa, 1997; McIntyre and Grill, 2002), Ia-inhibitory interneurons, group-II excitatory interneurons, and group-Ia and group-II afferents (Figure 1A). To simulate serotonin-mediated modulation of motoneuron membrane dynamics that is required to enable locomotion in rats with SCI (Courtine et al., 2009), we reduced the conductance of potassium-calcium gated ion channels in the model (Booth et al., 1997).

Second, we estimated the time profiles of firing rates of group-Ia and group-II afferent fibers during gait using a muscle spindle model (Prochazka and Gorassini, 1998a, 1998b) and a validated biomechanical model of the rat hindlimb (Johnson et al., 2011). We recorded joint trajectories during locomotion in healthy rats and estimated muscle stretch profiles of flexor (tibialis anterior) and extensor (gastrocnemius medialis) muscles of the ankle through inverse kinematics (Figure 1B).

Third, we modeled the interactions between the natural firing rate of efferent and afferent fibers and the depolarization elicited by EES pulses. These interactions are non-linear, since EES-induced depolarization may fail to elicit action potentials if the stimulation collides with ongoing depolarization or refractory state (Figures 1C and S1). To account for this non-linearity, we computed the membrane summation of natural and EES-induced depolarization for each simulated fiber. Estimates of the percentage of recruited fibers were derived from our validated finite element model of EES (Capogrosso et al., 2013).

Fourth, we converted efferent firing rates into electromyographic (EMG) activity by convolving wavelets of Gaussian-distributed amplitudes and durations with population of action potentials (Figure S1D).

Validation of the Muscle Spindle Feedback Circuit Model

To validate the predicted interactions between EES and the neuronal network, we assessed whether the model was able to qualitatively replicate the spinal reflex recruitment curves elicited by EES (Gerasimenko et al., 2006). We simulated the recruitment of afferent and efferent fibers in response to single EES pulses of increasing intensity and computed motor responses evoked in ankle muscles. We then compared simulations with experimental recordings in rats (n = 3). Until half the saturation range, EES only elicited medium- and late-latency motor responses through the recruitment of afferent fibers (92% energy of medium responses in simulations; 96% ± 2% in experiments). The shape, latency, and modulation of these responses exhibited qualitative similarities in the model and in vivo (Figure 1E). At higher intensities, EES additionally recruited efferent fibers, which led to the progressive decrease and eventual suppression of medium- and late-latency motor responses, both in the model and in vivo (66% energy of early responses in simulations; 67% ± 20% in experiments).

Impact of EES on Efferent and Afferent Fibers

We then exploited the computational model to study the impact of EES frequency and amplitude on the firing rate of afferent and efferent fibers during locomotion.

We found that increments in frequency ranging from 10 to 100 Hz led to a linear increase in the mean firing rate of group-Ia and group-II afferents (Figure 2A; R^2 = 0.99 for extensors and flexor). A comparable modulation was observed when increasing EES amplitude from 0.8 to 2 times the motor threshold, although the responses rapidly reached saturation due to the recruitment of all fibers. In all conditions, however, the temporal profiles of afferent firing rates were preserved, indicating that EES does not interfere with the natural encoding of locomotor-related information.

The integration of afferent firing rates into the neuronal network led to reciprocal activation of extensor and flexor motoneurons during specific phases of gait (Figures 2B and S2). Increments in EES frequency mediated a linear increase in the firing rates of both extensor (R^2 = 0.99) and flexor (R^2 = 0.93) motoneurons. Due to reciprocal inhibitory networks, this modulation only occurred during the phase corresponding to the natural recruitment of motoneurons (Figure S2), regardless of EES frequency. In contrast, increasing EES amplitude recruited the axons of motoneurons, including during the inactive phase, which disrupted the natural alternation between extensor and flexor (Figure 2B).

Dynamic Validation of the Computational Model

We tested whether the model was able to predict the modulation of muscle activity mediated by varying EES frequencies and amplitudes during gait, and under different conditions of standing and walking. For stimulation values normally used during experimental recordings (40 Hz frequency, 1.2 motor threshold amplitude), the model generated reciprocal bursts of modulated electromyographic activity in extensor and flexor muscles that matched experimental observations in rats with complete SCI (r = 0.86 and 0.85 for extensors and flexors; Figure 2C). These bursts were composed of modulated medium- and late-latency
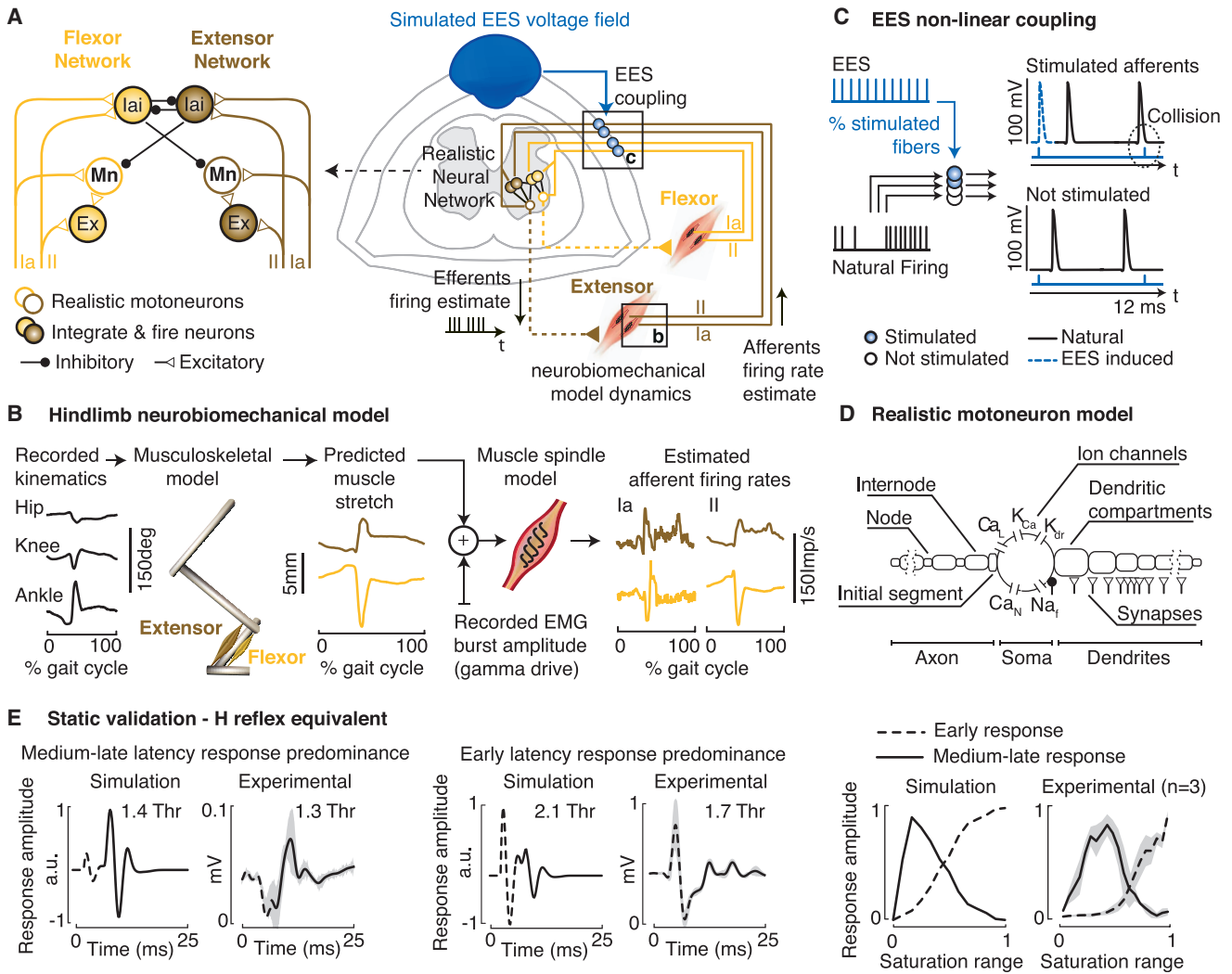
A

Flexor Network   Extensor Network

Iai   Iai

Mn   Mn

Ex   Ex

Ia II   II Ia

○ Realistic motoneurons
◉ Integrate & fire neurons
●— Inhibitory   ◁ Excitatory

Simulated EES voltage field

EES coupling

Realistic Neural Network

c

Flexor
Ia
II

Extensor
II
Ia

b

Efferents firing estimate
t

neurobiomechanical model dynamics

Afferents firing rate estimate

C   EES non-linear coupling

EES

% stimulated fibers

Natural Firing

○ Stimulated
○ Not stimulated

Stimulated afferents
100 mV
Collision
t

Not stimulated
100 mV
12 ms
t

—— Natural
---- EES induced

B   Hindlimb neurobiomechanical model

Recorded kinematics → Musculoskeletal model → Predicted muscle stretch — Muscle spindle model → Estimated afferent firing rates

Hip
Knee
Ankle
150deg
0   100
% gait cycle

Extensor
Flexor

5mm
0   100
% gait cycle

+

Recorded EMG burst amplitude (gamma drive)

Ia   II
150Imp/s
0 100 0 100
% gait cycle

D   Realistic motoneuron model

Ion channels
Internode
Node
Dendritic compartments
Ca_L K_Ca K_dr
Initial segment
Ca_N Na_f
Synapses

Axon   Soma   Dendrites

E   Static validation - H reflex equivalent

Medium-late latency response predominance

Simulation
1.4 Thr
Response amplitude a.u.
1
-1
0 Time (ms) 25

Experimental
1.3 Thr
0.1
mV
0
0 Time (ms) 25

Early latency response predominance

Simulation
2.1 Thr
Response amplitude a.u.
1
-1
0 Time (ms) 25

Experimental
1.7 Thr
1
mV
0
0 Time (ms) 25

- - - - Early response
—— Medium-late response

Simulation
Response amplitude
1
0
0   Saturation range   1

Experimental (n=3)
1
0
0   Saturation range   1

Figure 1. Computational Model of Muscle Spindle Feedback Circuits

(A) Biologically realistic neural network of muscle spindle feedback circuits for two antagonist muscles.

(B) Musculoskeletal model of the rat hindlimb, prediction of the muscle stretch during locomotion for antagonist ankle muscles, and resulting firing rates using a muscle spindle model.

(C) Modeling of nonlinear interactions between natural firing rates along afferent fibers and depolarization induced by EES.

(D) Realistic motoneuron model.

(E) Motor responses evoked in ankle muscles when delivering a single pulse of EES at various intensities expressed with respect to the motor threshold (Thr) in the model and experimentally. Plots report the modulation (±SEM) of motor responses with increasing EES intensities, expressed as percent of the saturation level.

responses that were locked to each pulse of EES (Figure S3A). A 2-fold increase in EES frequency induced a higher density of responses, which augmented the overall muscle activity (25% ± 8% for extensors and 27% ± 7% for flexors in the model versus 29% ± 15% for extensors and 33% ± 16% for flexors in vivo, n = 55 steps; Figure S3B). However, the reciprocal activation between antagonist muscles remained unaffected, both in the model and in vivo (Figure 2C). Increasing EES amplitude led to co-activation of extensor and flexor muscles, as observed in simulations.

EES enables spinal circuits isolated from supraspinal inputs to use sensory information as a source of control to produce motor patterns for standing and walking at different speeds (Courtine

et al., 2009). The model reproduced the differential modulation of burst durations in extensor and flexor muscles with increasing treadmill velocities and during transitions from walking to standing (Figure 2D; Movie S1). These combined results support the validity of our model and suggest that EES modulates muscle spindle feedback circuits to facilitate the alternating recruitment of antagonist motor pools in the absence of supraspinal input.

Exploiting Spinal Circuit Dynamics to Target Distinct Muscle Spindle Feedback Circuits with EES

Simulations show that reciprocal inhibition restricts the effects of EES to the phase during which motoneurons are recruited
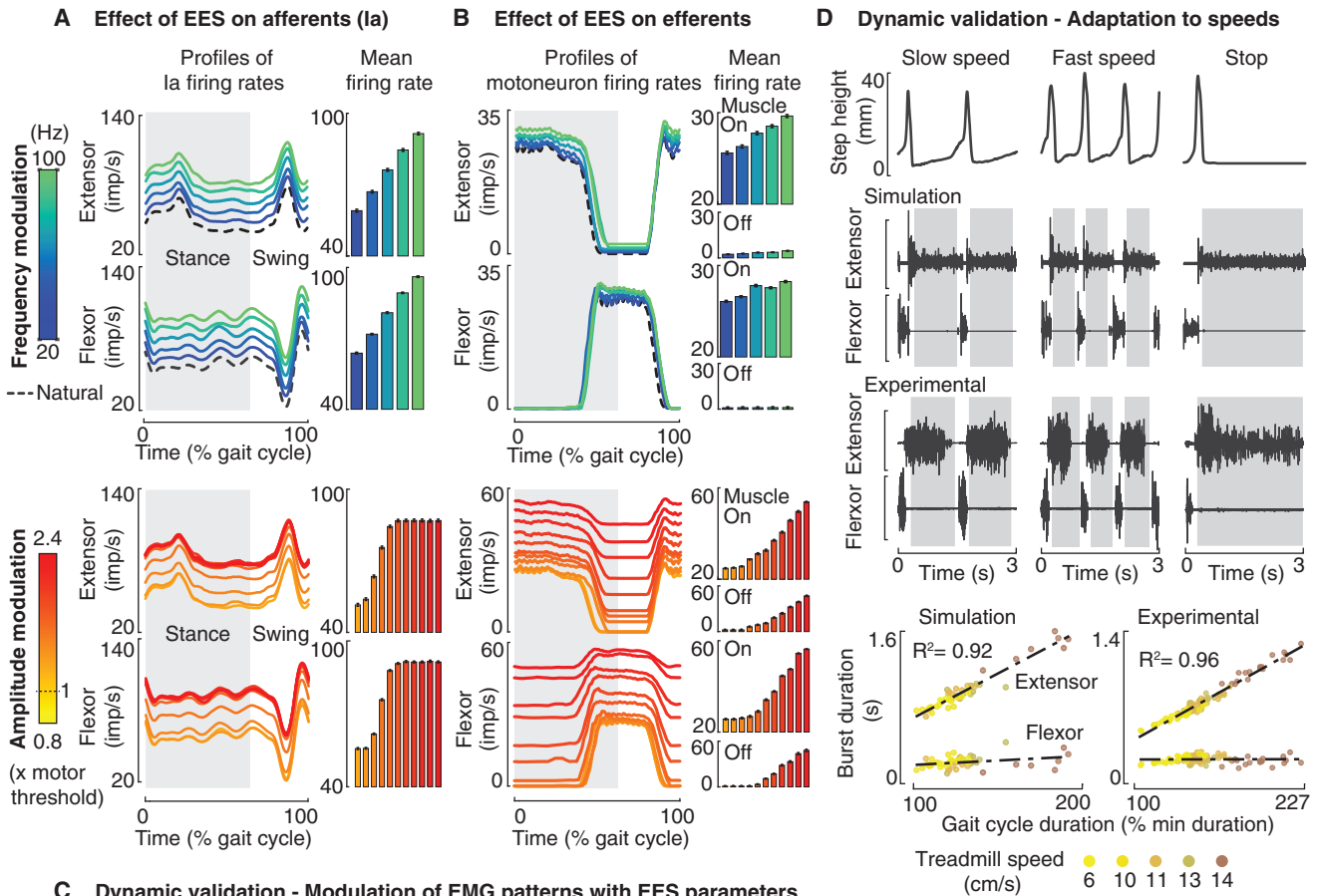
Figure 2. Interactions between EES and Spinal Circuit Dynamics during Locomotion

(A) Estimated firing rate along group-Ia fibers over the gait cycle under different EES frequencies (top) and amplitudes (bottom). Shaded areas indicate phases of extensor activity (stance). Bar plots report the mean (±SEM) firing rates computed over ten simulated gait cycles.

(B) Estimated firing rate along efferent axons under the same conditions as in (A). Bar plots report the mean (±SEM) firing rates over ten simulated gait cycles for each motor pool. The ON/OFF phases of each muscle were defined as the time period when motoneuron activity was higher/lower than one SD from the maximum.

(C) Simulated and experimental muscle activity patterns during locomotion under different EES frequencies and amplitudes.

(D) Simulated and experimental muscle activity patterns during locomotion under different treadmill speeds and during the transition from stepping to standing. Plots report the relationships between gait cycle duration and burst duration of flexor and extensor muscles derived from simulations and experimental recordings.

(Figures 2B, S3, and S4). This result suggests that phase-dependent modulation of muscle spindle feedback circuits filters the effects of EES toward functionally relevant pathways. We hypothesized that this property may be exploited to selectively modulate flexor versus extensor muscles through phase-specific adjustment of EES. We performed simulations in which EES frequency was independently tuned during stance versus swing phases. These simulations revealed that phase-specific EES gradually and specifically modulates the activity of extensor versus flexor muscles (Figures 3A and S4A).
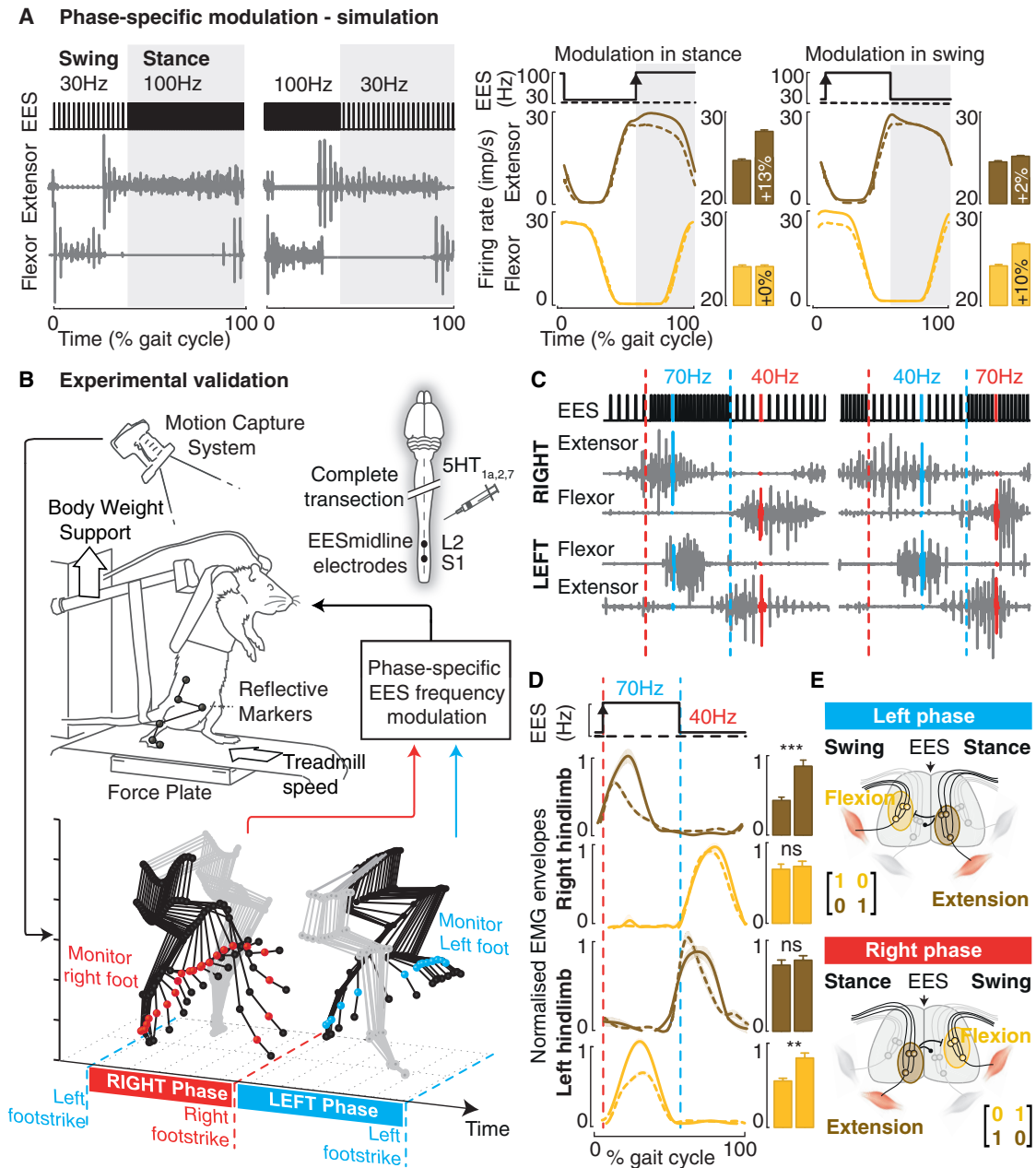
Figure 3. Phase-Specific Modulation of EES Frequency during Gait

(A) Simulated EMG patterns and estimated firing rates along efferents during locomotion while EES frequency varies during stance or swing. Conventions are the same as in Figure 2. Bar plots report the mean (±SEM) firing rates over ten gait cycles for each motor pool.

(B) Experimental platform for phase-specific modulation of EES frequency based on movement feedback in rats with complete SCI. Real-time monitoring of hindlimb kinematics automatically detected left and right foot strikes, which segmented gait cycles in two phases.

(C) Muscle activity patterns during stepping under phase-specific EES, together with train of stimulation pulses.

(D) Rectified muscle activity (continuous lines) recorded during locomotion with phase-specific modulation of EES frequency, compared to continuous EES (40 Hz, dashed lines). Bar plots report the mean (±SEM) activity of each muscle during continuous (left) versus phase-specific (right) EES (n = 4 rats).

(E) Scheme and matrix formulation illustrating the natural gating of muscle spindle feedback circuits during locomotion, which filter the effects of EES toward active muscles (2 × 2 matrices, input stimulation spatial specificity, and output functional specificity).

We tested whether the same specificity was obtained in rats with complete SCI. The combination of a serotonin replacement therapy and midline EES enabled locomotion in all rats (Courtine et al., 2009). We expanded our real-time stimulation platform (Wenger et al., 2014) to enable closed-loop adjustment of EES parameters based on bilateral hindlimb kinematics. Automated
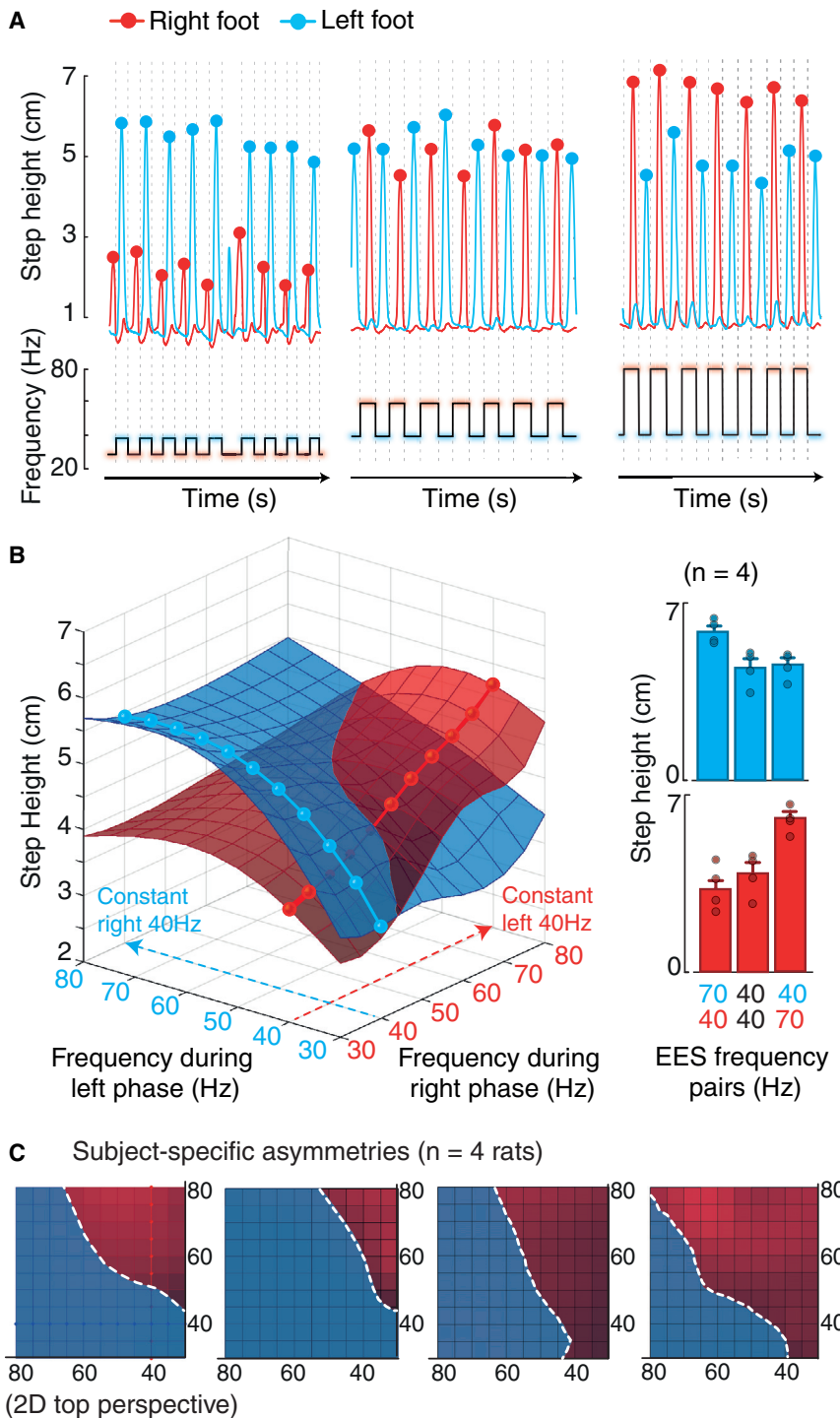
Figure 4. Phase-Specific Adjustment of EES Frequency Independently Modulates Bilateral Foot Trajectories in Rats with Complete SCI

(A) Vertical displacements of the left and right feet during locomotion under three patterns of phase-specific EES frequencies. EES frequency was adjusted during the right phase (30 Hz, 60 Hz, and 80 Hz), while EES remained unchanged on the left phase for all three protocols. The dots and dashed vertical lines highlight maximum foot heights and foot strike events, respectively.

(B) 3D plot showing the relationships between maximum left and right step heights and phase-specific EES frequencies (>850 step cycles covering the entire input space). Bar plots highlight side-specific modulations across animals (n = 4).

(C) 2D projections of the same representation as in (B) for each tested rat. The white dotted line indicate the intersection between both surfaces, highlighting the pairs of phase-specific EES frequencies that would theoretically induce symmetry for each rat.

validated these predictions. We found a linear relationship between EES frequency and the amplitude of ipsilateral extensor and contralateral flexor muscles (Figures 3C, 3D, and S4B). These effects were restricted to the period during which muscles were active, confirming the ability of phase-specific EES to modulate distinct spinal circuits during gait.

Model-Derived Control Policies Modulate Bilateral Hindlimb Movements during Locomotion

We next sought to leverage these properties to develop control policies that actively tune left versus right hindlimb movements during locomotion. We conducted a comprehensive mapping of changes in left and right step heights for pairs of EES frequencies ranging from 20 to 80 Hz, which we represented in a 3D space (n > 300 steps per rat; Figures 4B and S5). Each hindlimb displayed a linear relationship between step height and phase-specific EES frequency, which was independent of the contralateral hindlimb. Consequently, the modulation for each hindlimb laid on a planar surface

detections of foot strikes divided gait into interleaved left and right phases (Figure 3B). During stepping, extensor muscles of one hindlimb are active at the same time as flexor muscles of the other hindlimb (Figure 3C). Consequently, model predictions suggested that changes in EES frequency during the left-stance phase would simultaneously modulate left extensor and right flexor muscles and inversely for the right-stance phase. Experimental recordings

(Figure 4B). These planes quantified the degree of asymmetry between the left and right steps, while their intersection defined the pairs of EES frequency that are theoretically appropriate to correct these idiosyncratic deficits (Figure 4C).

To test this possibility, we embedded a control structure within the real-time stimulation platform, composed of two controllers interleaved in time. Each controller monitored the foot trajectory
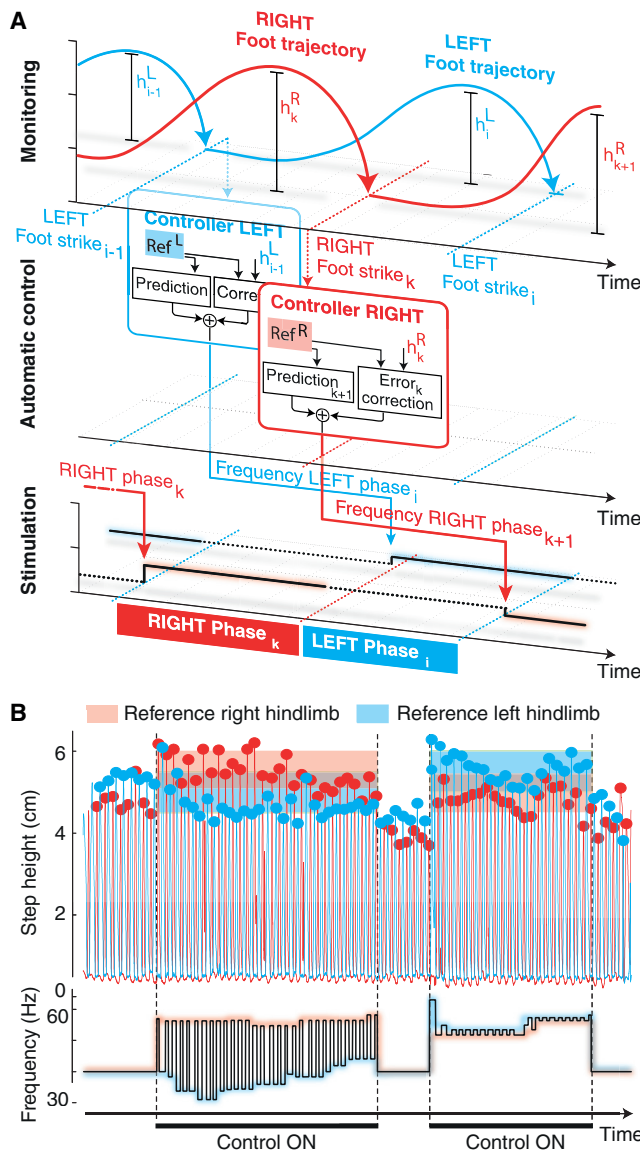
Figure 5. Real-Time Control of Bilateral Step Height during Locomotion in Rats with Complete SCI

(A) Closed-loop control structure composed of two independent controllers, one for each hindlimb, operating in parallel. Each controller combines a forward model and a proportional integral controller that calculate corrections of EES frequency during the phase *k* in order to maintain the maximum step height (h_k^R and h_k^L for right and left hindlimbs) within a predefined reference band (Ref^L and Ref^R). Corrections in EES frequency are applied at the next iteration of the same phase (*k + 1*).

(B) Continuous sequence showing the controllability of step heights for the left and right hindlimbs with phase-specific EES frequencies. The left and right controllers target step height reference bands (shaded areas) that were inverted between the first and second controlled periods.

of one hindlimb and adjusted EES frequency during its swing phase to target a desired step height, regardless of the other limb (Figure 5A). We thus capitalized on phase-dependent modulation of spinal circuits to control a single-input multiple-output (SIMO) system out of two independent controllers operating in

parallel. To evaluate the performance of this control structure, we applied sudden changes in the desired step height for each hindlimb independently (Figures 5B and S6B). For each task, the controllers successfully adjusted phase-specific EES frequencies to target the desired step height of each hindlimb with high precision (error <5 mm), even when imposing references reaching the physiological limits of motion (Figure S6B). More complex feed-forward predictive models that implicitly account for time and interlimb effects required longer convergence times and failed to improve performance (Figure S6C).

Model-Derived Control Policies Restore Symmetry and Improve Balance

We next tested whether closed-loop control of phase-specific EES frequencies is able to correct idiosyncratic deficits of gait and balance. Each injured rat exhibited a distinct degree of asymmetry that altered interlimb coordination and balance, primarily due to discrepancies in the recruitment of extensor muscles (Figure 6A). We configured the controller to maintain left and right steps at the same height. Corrections in EES frequency during the stance phase of the weaker hindlimb augmented extensor muscle activity and promoted whole-limb extension. This tuning reestablished symmetry and distributed vertical ground reaction forces equally in all tested rats (p < 0.001 for each rat; Figure 6A; Movie S3). The controller converged toward EES frequency pairs that scattered along the symmetry line defined by the intersection of the correlation planes (Figure 6B). These adaptions also restored balance. During controlled conditions, the center of pressure displayed oscillations centered on the body midline, which contrasted with the pronounced lateral shifts underlying non-controlled steps (p < 0.001; Figure 6C). Moreover, the distribution of ground reaction forces was less variable during controlled compared to non-controlled steps (p < 0.001).

Model-Derived Control Policies Improve Locomotor Performance

We then evaluated whether the controller was able to maintain gait performance while increasing weight-bearing levels and speeds, two behavioral conditions that involve enhanced physical effort. During non-controlled steps, reduction of body-weight support led to a decrease in step height and extension, together with increased variability (Figure 7A). The controller adjusted EES frequency to preserve left and right foot elevation. Tuning of EES frequency reinforced the activity of extensor muscles, which resulted in larger vertical ground reaction forces that enabled the rats to sustain increased loads equivalent to 15% of their body weight (Figure 7A; Movie S4).

During transitions from normal to high speeds, injured rats exhibited an increase in backward foot movements during stance and pronounced dragging during swing, which reflected their difficulties to meet task requirements (Figure 7B). The controller adjusted EES frequencies to alleviate these deficits (p < 0.01 for each rat).

Model-Derived Control Policies in Clinically Relevant Rodent Models

Finally, we sought to evaluate the translational potential of phase-specific EES protocols. SCI in humans primarily results
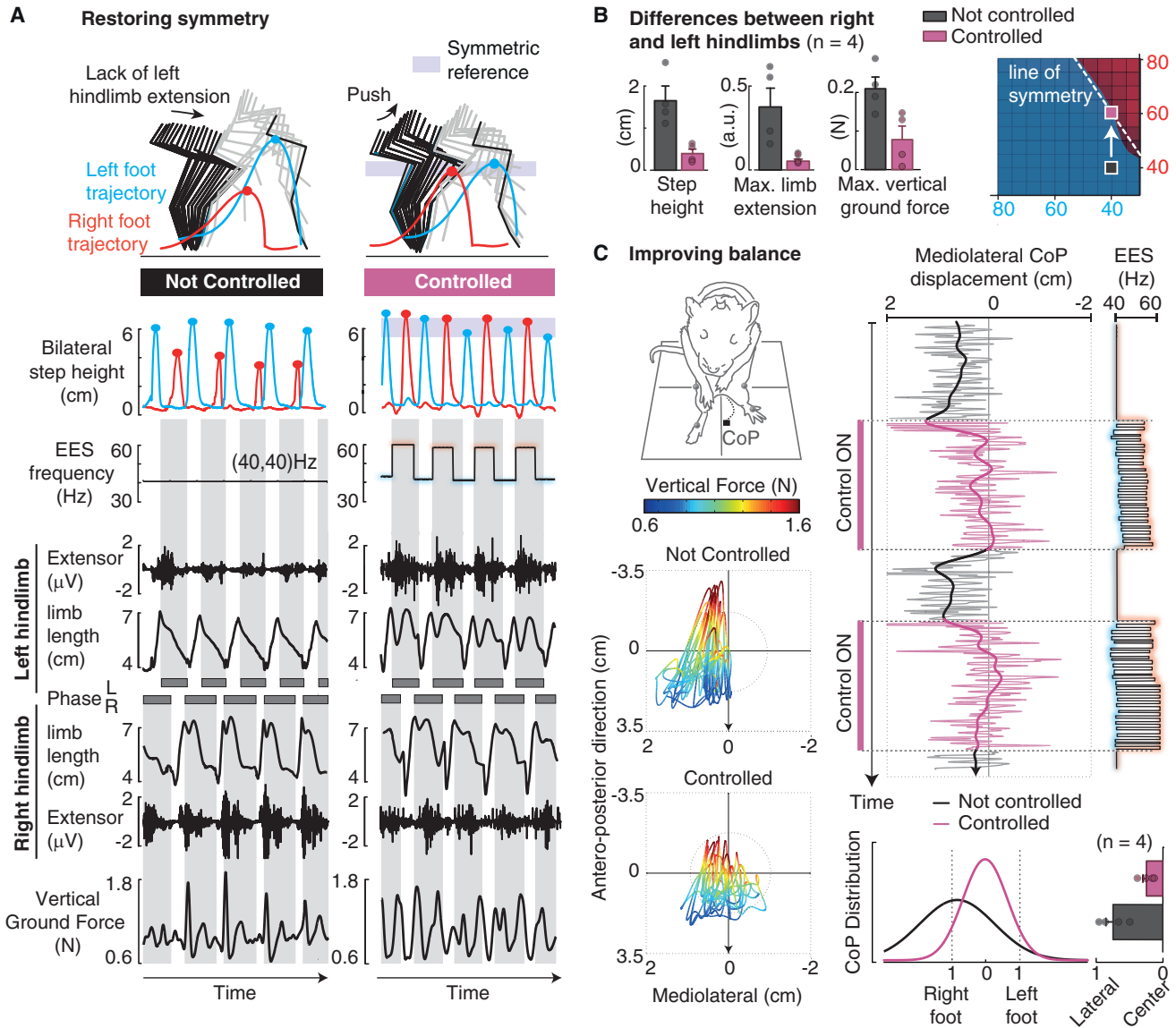
Figure 6. Closed-Loop Control of Phase-Specific EES Frequency Restores Symmetry and Balance in Rats with Complete SCI

(A) Decomposition of left hindlimb kinematics and trajectories of the left and right feet under non-controlled and controlled conditions. The vertical displacements of both feet are displayed together with concurrent changes in EES frequency, EMG activity of left and right extensor muscles, and bilateral hindlimb length during a non-controlled and controlled sequence. Boxes indicate left (L) and right (R) stance phases.

(B) Bar plots reporting mean differences (±SEM) between the left and right hindlimbs for relevant gait features during non-controlled and controlled conditions. Single dots refer to individual rats. The controller selected pairs of EES frequencies that converged toward the theoretical line of symmetry.

(C) Center of pressure (CoP) displacement and color-coded vertical ground reaction forces during locomotion. The origin indicates the equidistant position of the CoP between both feet during standing. Continuous changes in mediolateral CoP displacements are shown together with phase-specific EES frequencies during a sequence alternating non-controlled and controlled conditions.

from contusion injuries, which lead to variable damage. Consequently, these lesions induce a broad spectrum of asymmetries in gait deficits (Friedli et al., 2015). Moreover, the severity and specificity of the SCI is likely to determine the appropriate level of serotoninergic replacement therapies to facilitate gait.

To address these issues, we first studied whether the modulation of muscle activity with EES frequency was preserved in the absence of serotoninergic replacement therapies. We withdrew

serotonin-mediated modulation of motoneuron membrane dynamics in the model (Figure 8A). Simulations showed that the absence of serotonin reduced muscle burst amplitude, but did not affect the alternation between extensor and flexor muscles. Moreover, the modulation of muscle activity during changes in EES frequency was preserved, which compensated for the withdrawal of serotonin (Figure 8A). To validate these results, we placed a lateralized contusion SCI that induced different degrees
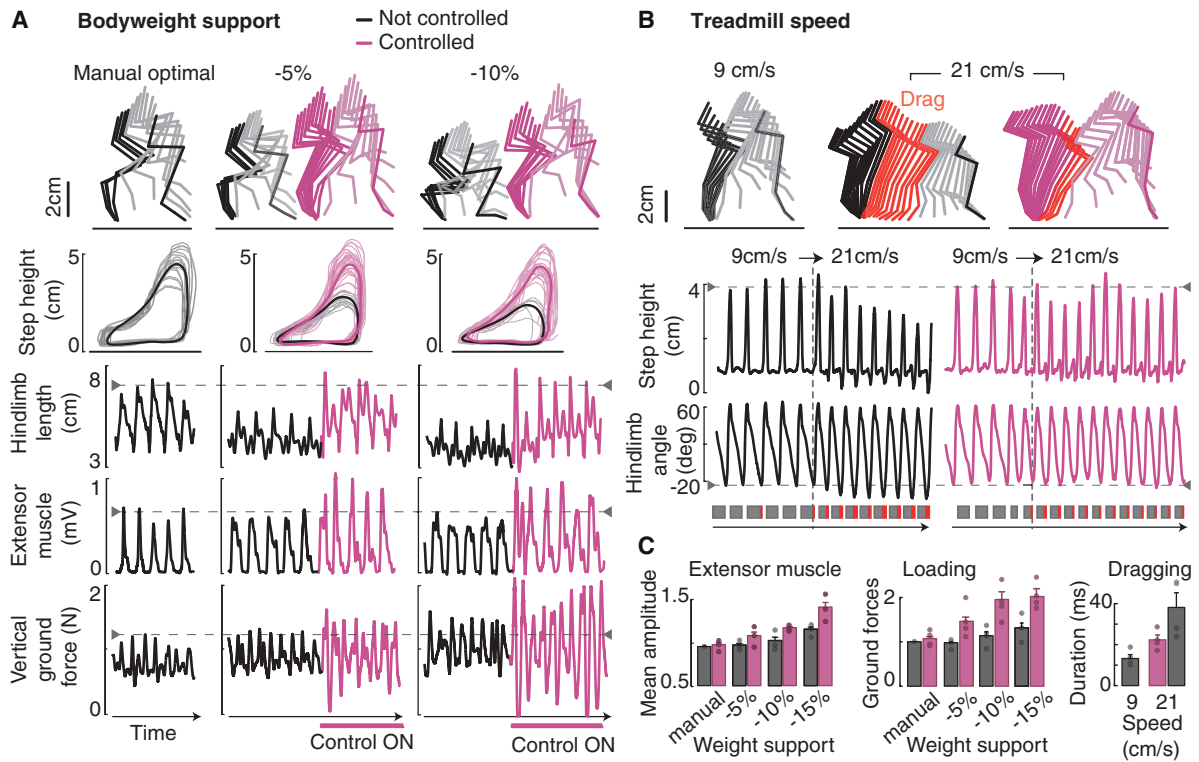
Figure 7. Closed-Loop Control of Phase-Specific EES Frequency Preserves Stepping Performance during Tasks Requiring Enhanced Physical Effort

Rats with complete SCI were tested in two challenging tasks under non-controlled versus controlled conditions.

(A) Decomposition of hindlimb kinematics, foot trajectories, and continuous changes in hindlimb length, extensor muscle activity, and vertical ground reaction forces during locomotion under progressive decrease in body-weight support.

(B) Decomposition of hindlimb kinematics and continuous changes in vertical foot displacement and hindlimb angle during locomotion during the transition from slow to fast stepping. The controller progressively reinforced the amplitude of muscle activity, which enhanced weight-bearing levels while maintaining stepping consistency and minimizing dragging.

(C) Bar plots report mean values (±SEM, n = 4 rats) of relevant gait parameters during decrease in body-weight support and increase in speed. Single dots refer to individual rats.

of gait asymmetry and deficits (Figures 8B, 8C, and S7). Without serotonin, EES promoted locomotion in all tested rats despite a significant decrease in muscle activity (p < 0.05; Figure 8B). As observed in the model, the tuning of muscle activity and hindlimb kinematics was conserved during changes in EES frequency, which robustly modulated hindlimb movements.

We then personalized the serotoninergic replacement therapy for each rat and tested whether phase-specific EES frequency was able to correct gait asymmetry and subject-specific deficits. While rats exhibited markedly different alterations, phase-specific EES frequency restored symmetry and improved hindlimb kinematics in all tested rats (p < 0.001; Figure 8C; Movie S3).

DISCUSSION

EES of lumbar segments is undergoing a rapid transition from animal models to clinical applications (National Institutes of Health, 2015). This transition requires a conceptual framework that guides the implementation and optimization of this intervention. Here, we derived stimulation protocols addressing subject-specific gait impairments from the identification of computational mechanisms underlying motor pattern formation during EES. This approach opens new perspectives for hypothesis-driven optimization of EES protocols. We discuss these findings with an emphasis on the computational mechanisms of EES, how this understanding can steer the design of ecological stimulation protocols, and their relevance for clinical applications.

Mechanisms Underlying Motor Pattern Formation during EES

Simulations (Capogrosso et al., 2013; Rattay et al., 2000) and experimental studies (Gerasimenko et al., 2006; Hofstoetter et al., 2015) have provided evidence that EES primarily engages large-diameter afferent fibers. The prevailing view is that the recruitment of these afferents activates central-pattern generating networks (Angeli et al., 2014; Danner et al., 2015) and raises the excitability of spinal circuits to a level that enables sensory information to become a source of motor control (Edgerton et al., 2008). Despite the wide acceptance of this interpretation, the principles from which the recruitment of afferents fibers
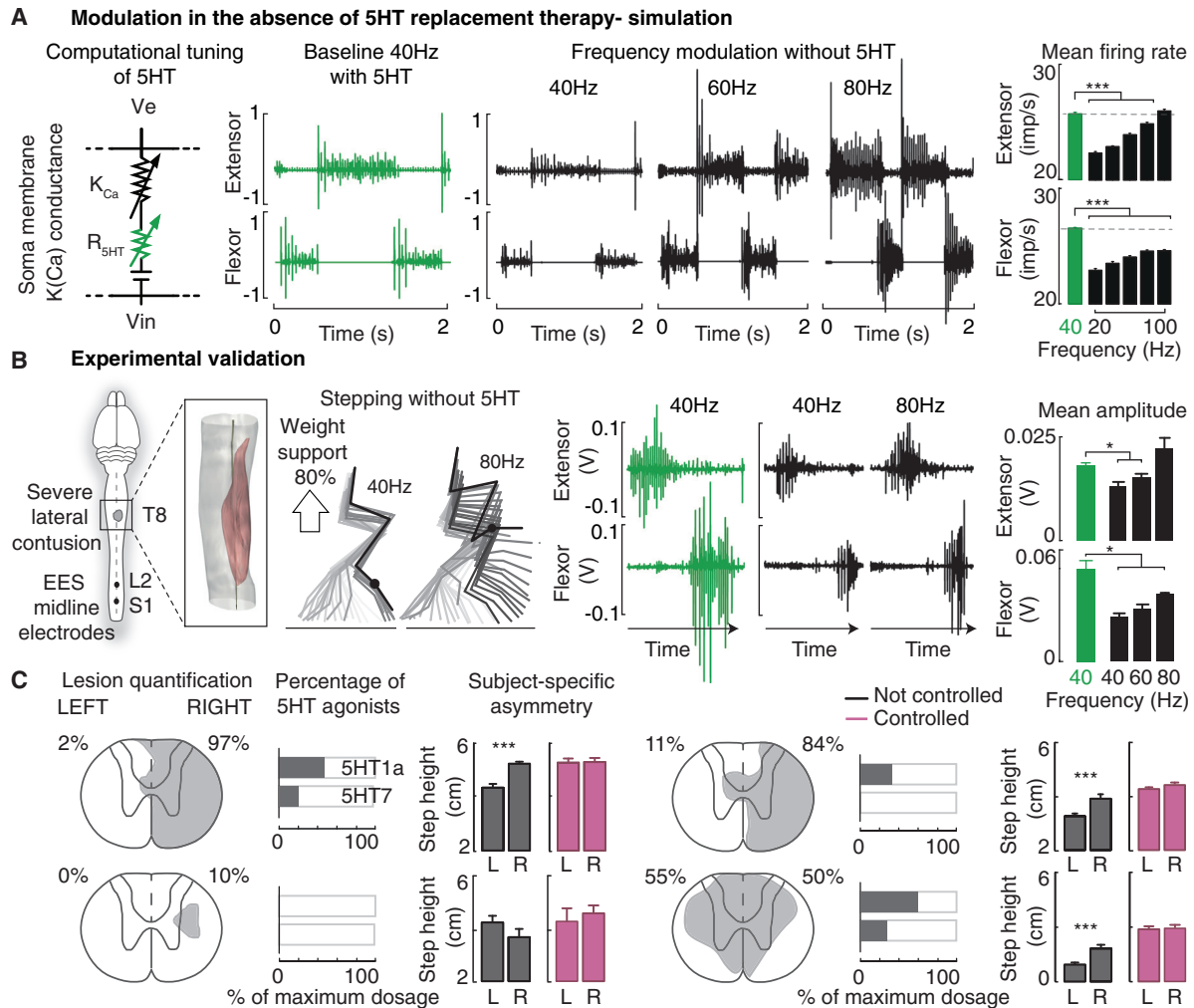
Figure 8. Phase-Specific EES Frequency in Rats with Clinically Relevant SCI under Minimal Serotonin Replacement Therapy
(A) Model of 5-HT mediated tuning of motoneuron soma membrane conductance. Simulated muscle activity patterns during locomotion with 5-HT and without 5-HT under different EES frequencies. Bar plots report mean firing rates along efferent axons computed over 10 gait cycles per EES frequency. Increase in EES frequency compensated for the lack of 5-HT.
(B) 3D reconstruction of a lateralized contusion SCI. Decomposition of hindlimb kinematics under two distinct EES frequencies. Muscle activity patterns recorded in a rat with a contusion SCI under the same conditions as in (A), including quantifications of muscle activity across the four tested rats.
(C) Reconstruction of damaged tissue (shaded area, including percent) on each hemicord for each rat. Horizontal bar plots report the optimal 5-HT agonist dosage for each rat, expressed in percent of the maximum dosage necessary for rats with complete SCI. Bar plots report mean values (±SEM) of left (L) and right (R) step heights under non-controlled and controlled conditions for each rat. ***p < 0.001, unpaired t test. The controller restored symmetry in all the rats, regardless of idiosyncratic motor deficits and the level of 5-HT agonist concentration.

translates into organized patterns of muscle activity has remained enigmatic. Here, we show that EES modulates muscle spindle feedback circuits and interacts with natural sensory information to elaborate and tune motor patterns for standing and walking at different speeds. Simulations integrating muscle spindle feedback circuits and reciprocal inhibitory networks were sufficient to reproduce a broad range of task-specific motor patterns that resembled those recorded experimentally in rats with SCI.

Dynamic simulations allowed us to probe the interactions between EES and each component of the modeled spinal circuits. We found that EES uniformly enhances the activity along muscle

spindle feedback pathways throughout the duration of the gait cycle. Nevertheless, this global increase in afferent firing rates does not alter the natural information encoded in the temporal profile of muscle spindle firing. The interactions between EES and natural muscle spindle activity engage two synergistic mechanisms. First, the recruitment of muscle spindle feedback circuits provides a mono- and di-synaptic excitatory drive to motoneurons. Second, the strengthening of reciprocal inhibition between antagonist motor pools promotes the alternative recruitment of extensor and flexor muscles (Jankowska, 1992; Talpalar et al., 2011). In turn, the natural sensory input related to hindlimb movement modulates the balance between these

two mechanisms, which gates the flow of information toward functionally relevant pathways (Tripodi et al., 2011). Thus, sensory information acts as the source of control that steers the production of versatile motor patterns without supraspinal input (Courtine et al., 2009; Edgerton et al., 2008). For example, changes in sensory information tuned extensor burst duration for different treadmill speeds while preserving flexor burst duration, as reported experimentally (Rossignol et al., 2006). Likewise, stopping the treadmill prolonged the activity of extensor muscles while inhibiting flexor muscles, which promoted an immediate transition from walking to standing (Quevedo et al., 2000). Our computational model based on muscle spindle feedback circuits was sufficient to explain the production of these complex motor behaviors. While other mechanisms including central pattern generator networks may also contribute to the observed locomotor activities (Rybak et al., 2006), the present results reinforce current views on the predominant role of sensory information for the production of complex and adaptive motor behaviors in the absence of supraspinal drive in mammals (Ekeberg and Pearson, 2005; Song and Geyer, 2015).

Hypothesis-Driven Stimulation Protocols Manipulating Circuit Dynamics to Improve Gait

Computational models provide access to the detailed and global properties of circuit dynamics, supporting the formulation of novel hypothesis-driven neuromodulation therapies (McIntyre and Foutz, 2013). Our simulations led to the hypothesis that phase-specific adjustment of EES frequency would independently modulate the bilateral activity of active muscles during locomotion. We found that the filtering properties of spinal circuits ensure that frequency-mediated modulation of muscle activity is selectively directed toward functionally active muscles. Therefore, phase-specific EES frequency provides the opportunity to tune bilateral motor patterns without disrupting the natural alternation between antagonist motor pool recruitment. The experimental implementation of this neuromodulation strategy corrected gait deficits and improved balance in rats with complete and incomplete SCIs. This bilateral modulation emerged from the natural gating of muscle spindle feedback circuits, which augmented extensor muscle activity on one hindlimb while concurrently enhancing flexor muscle activity on the other hindlimb. Phase-specific modulation of EES frequency thus harnesses the fundamental properties of spinal circuit dynamics to modulate bilateral leg movements. On the contrary, increases in EES amplitude additionally recruited efferent fibers directly, thus bypassing the filtering properties of spinal circuits and disrupting phase-dependent modulation of antagonist motoneurons. Phase-specific manipulation of EES parameters thus enables ecological interactions with the natural operations of spinal circuits (Courtine and Bloch, 2015).

This hypothesis-driven stimulation protocol steered the design of a minimal but effective closed-loop control policy that only necessitates a single input to trigger precise adjustments of bilateral movements. The controller monitored a single feature for each hindlimb, which was sufficient to capture changes in bilateral kinematics. This neuromodulation strategy required no manual tuning yet mediated robust adjustments of hindlimb movements and balance through personalized therapies targeting subject-specific motor deficits.

Conservation of Spindle Feedback Circuits across Mammals Supports Clinical Translation

Repetitive activation of motor circuits during rehabilitative training promotes activity-dependent plasticity of spinal circuits that improves functional recovery after SCI (Borton et al., 2013). Experiments in animal models and human patients showed that task-specific features such as weight-bearing levels, walking speed, gait symmetry, and balance play a key role in determining the kind and extent of motor improvements (Barbeau et al., 1999; Edgerton et al., 2008). Commonly, physical therapists seek to optimize these components through manual assistance (Dietz et al., 1998). Our control strategy effectively targeted all these gait features. Closed-loop neuromodulation therapies automatically improved gait execution in rats with both complete and incomplete SCI, regardless of the amount of residual supraspinal control and/or levels of serotonergic replacement therapy. These synergistic interactions were possible because our model-derived control strategies manipulate muscle spindle feedback circuits, which are the building blocks engaged by both sensory information and supraspinal commands to elaborate motor patterns (Arber, 2012; Levine et al., 2014). Electrophysiological evidence indicates that these ancestral components of the vertebrate motor infrastructure (Clarac et al., 2000; Sherrington, 1910), which are remarkably conserved across mammals (Pierrot-Deseilligny, 1989), are also recruited by EES in humans (Hofstoetter et al., 2015; Sayenko et al., 2014). These results suggest that the manipulation of muscle spindle feedback circuits with EES have the potential to alleviate leg motor deficits in human patients with SCI.

Limitations and Future Perspectives

The electrophysiological signature of motor responses elicited in leg muscles after each pulse of EES suggested that this stimulation primarily engages large-diameter myelinated fibers, in particular muscle spindle feedback circuits (Capogrosso et al., 2013; Gerasimenko et al., 2006; Wenger et al., 2014). Therefore, we restricted our model to these pathways. However, gravity strongly influences the control and modulation of locomotion, especially in humans (Cavagna et al., 2000; Lacquaniti et al., 2012; Pearson, 1993). Golgi tendon organs and skin mechanoreceptors are the main sensory receptors providing gravity-related information to spinal circuits (Capaday, 2002). The inclusion of these pathways is thus a prerequisite to implement realistic forward biomechanics in our model. These pathways will also be critical to dissect the role of individual spinal circuits in the production of locomotion, including central pattern generating networks.

Here, we used our computational framework to develop a neuromodulation strategy that exploits temporal circuit properties to achieve functional specificity. Novel multi-electrode spinal implants (Minev et al., 2015) provide the opportunity to target subsets of muscle spindle feedback circuits, potentially supporting the development of spatially selective stimulation protocols. Thus, our computational model defines a framework to integrate spatial selectivity and temporal structure in neuromodulation

therapies that would take full advantage of the distributed building blocks underlying motor pattern formation.

Despite scientific and technological challenges, we believe that the marriage between computational modeling and tailored neurotechnologies will foster the optimization of stimulation protocols that mediate therapeutic effects in individuals with SCI.

EXPERIMENTAL PROCEDURES

Computational Model
Realistic Neural Network
The neural network is implemented in NEURON (Hines and Carnevale, 1997) using a parallel multi-threaded structure. Afferent fibers are modeled as Poisson point processes with average firing rates estimated from a spindle model and 20% noise level. The latency between action potentials and elicited excitatory postsynaptic potentials (EPSPs) to the target cell follows a normal distribution (mean = 2 ms, variance = 0.3 ms) accounting for the variability in afferents diameter. A total of 60 Ia- and group-II fibers are implemented for each motor pool (Segev et al., 1990). Each group-Ia fiber forms excitatory synapses to all motoneurons of the homonymous motor pool (Segev et al., 1990), while group-II fibers establish excitatory synapses onto each group-II interneuron (Stienen et al., 2007).

Each motor pool comprises 169 alpha motoneurons (Figure S1A) (Capogrosso et al., 2013; Jones and Bawa, 1997; McIntyre et al., 2002; Stienen et al., 2007). The membrane potential of each cell is described as a modified Hodgkin-Huxley model comprising sodium, potassium, calcium, and potassium-calcium gated ion channels (McIntyre et al., 2002). To model the effect of 5-HT agonists, which is used with EES to enable locomotion, we lowered the potassium-calcium gated ion channels conductance by 40% (Booth et al., 1997).

Motoneuron morphology consists of a 32- ± 10-μm-diameter spherical soma connected to an electronic-equivalent dendritic tree of mammalian S type alpha motoneurons (Fleshman et al., 1988; Jones and Bawa, 1997), dendritic sizes adapted to match soma diameter, from cell S-type cell 35/4. The initial segment and efferent axon are implemented with dedicated membrane dynamics (Capogrosso et al., 2013; McIntyre et al., 2002). Inhibitory synapses innervate the soma and behave as alpha functions with a reversal potential $E_{syn} = -75$ mV, a rise time constant $\sigma = 1.5$ ms, and a decay time constant $\tau = 2$ ms. The resulting inhibitory postsynaptic potential (IPSP) at the soma reaches an amplitude of -3 mV (McIntyre and Grill, 2002; Pratt and Jordan, 1987) (Figure S1B). Group-II interneuron excitatory synapses are located along the dendritic tree with a Poisson distribution (Jones and Bawa, 1997). Excitatory synapses are modeled by an exponential function with reversal potential $E_{syn} = 0$ mV and decay time constant $\tau = 0.5$ ms. The conductance of excitatory synapses from group-Ia fibers was tuned to a mean EPSP amplitude = 212 μV (Harrison and Taylor, 1981), increased by 28% to mimic the heteronymous contribution of synergistic innervations (Scott and Mendell, 1976). The conductance of group-II interneuron synapses was set to one-third the size of group-Ia fiber EPSPs to mimic the smaller impact of group-II fibers on motoneurons (Munson et al., 1980).

Excitatory and inhibitory interneurons were modeled as Integrate and fire cells with membrane time constant $\tau_m = 30$ ms. Due to the absence of experimental measurements, we tuned the strength of the reciprocal inhibition by comparing the energy of the simulated and experimental EMG signals. We computed a fitness score to measure the amount of alternation in bursting activity of antagonist motor pools during gait:

$$Alternation = mean(1 - (EMGenvelope_{flex} \cdot EMGenvelope_{ext}))$$

$$EnergyRatio = (EnergyEMGenvelope_{flex})/EnergyEMGenvelope_{ext} \cdot \\ (EnergyExperimetnalEMGenvelope_{ext})/EnergyExperimetnalEMGenvelope_{flex}$$

$$Fitness\ Score = Alternation \cdot EnergyRatio.$$

Synaptic strengths were set to match recordings in healthy rats during stepping (fitness score equal to 1). We performed a robustness test over the chosen value. A variation of 40% in IPSP conductance of Ia-interneurons induced a 37% change in fitness, compared to a total possible maximum change of 1,400% ranging from tonic activation to complete suppression of the motor pool activity. A variation of 56% in EPSP strength resulted in a 10% change in fitness score, showing that the chosen parameters are robust and preserve results over a wide range of values.

Muscle Spindles Model
Instantaneous firing rates of group-Ia and -II afferents fibers were computed using a spindle model (Prochazka and Gorassini, 1998a, 1998b). Fibers stretch and stretch velocity were linked to the envelope of EMG bursts to mimic the alpha-gamma linkage. The firing rates of the different fibers were computed using the following equations:

$$Ia\ firing\ rate = 50 + 2 \cdot stretch + 4.3 \cdot sign(strVelocity) \cdot |strVelocity|^{0.6} \\ + 50 \cdot EMG_{env}$$

(Equation 1)

$$II\ firing\ rate = 80 + 13.5 \cdot stretch + 20 \cdot EMG_{env}.$$ (Equation 2)

Biomechanical Model
Estimation of the muscle fiber stretch during gait was derived from a realistic musculoskeletal model of the rat hindlimb implemented in OpenSim (Delp et al., 2007) and validated experimentally (Johnson et al., 2011; Johnson et al., 2008). We fed OpenSim with crest, hip, knee, ankle, and metatarsophalangeal joint positions recorded in healthy rats (n = 10 steps) to calculate the corresponding muscle stretch profile of muscles of the ankle.

Coupling with EES
The number of fibers recruited by EES was computed using a validated finite element model of EES (Capogrosso et al., 2013) with the same geometry and parameters. The coupling between EES and the natural firing rate of afferent fibers is nonlinear. If a depolarization event occurs when the nodes of Ranvier are producing an action potential or during its refractory period, EES may fail to elicit a depolarization, or it may occur at higher thresholds. We modeled afferents fibers as integrate and fire cells with a membrane time constant = 30 ms. EES and natural firing rates were provided as suprathreshold synaptic inputs to each fiber. Firing rates were calculated from the sum of EES frequency and natural firing rate on the cell membrane.

EMG Model
Alpha motoneuron action potentials occurring at the last node of Ranvier were convolved with representative motor unit action potentials (MUAPs), modeled as damped sinusoidal waves with normally distributed amplitude (1 ± 0.2 a.u.) and duration (7.5 ± 2 ms) (Figure S1D). A latency of 2 ms between each event and the corresponding MUAP was implemented to account for the traveling time of an action potential from the spinal cord to the rat triceps surae (Gerasimenko et al., 2006).

Animals and Animal Care
All procedures and surgeries were approved by the Veterinarian Office Vaud, Switzerland. The experiments were conducted on 13 adult female Lewis rats (200 g body weight, Centre d'Elevage R. Janvier). Hindlimb kinematic and muscle activity during stepping were obtained in two healthy rats. Electrophysiology recordings were conducted in three rats. Behavioral experiments in eight rats with SCI. Rats were housed individually on a 12-hr light/dark cycle, with access to food and water ad libitum.

Surgical Procedures and Post-surgical Care
Procedures have been described in detail previously (Courtine et al., 2009; van den Brand et al., 2012). All interventions were performed under general anesthesia and aseptic conditions. Briefly, EMG electrodes were created by removing a small part (~1 mm notch) of insulation from a pair of Teflon-coated stainless steel wires inserted into the gastrocnemius medialis and tibialis anterior muscles of both hindlimbs. Stimulation electrodes (same type as EMG) were secured at the midline of the spinal cord at spinal levels L2 and S1 by suturing over the dura mater above and below the electrode. A common ground wire was inserted subcutaneously over the right shoulder. In the same surgery, the rats received a complete thoracic (T7) SCI (n = 4) or a lateralized contusion (250–300 KDyn) using the Infinite Horizon Impactor (n = 4). The extent and location of the lesions was verified postmortem on 20 equally spaced 40-μm-thick

transverse sections incubated in serum containing anti-GFAP (1:1,000, Z033429, Dako) antibodies. Contusion SCIs were reconstructed in 3D and the lesion extent expressed as a percentage of damaged tissue for each hemicord.

Locomotor Training and Recording

Rats were trained to step bipedally on a treadmill supported by a robotic body-weight support system (Robomedica). Training occurred every other day, for 20 min per session, for 4 weeks, starting 8 days post-SCI. 5HT1A/7 (8-OH-DPAT, 0.05–0.1 mg/kg body weight) and 5HT-2A/C (quipazine, 0.2–0.3 mg per kg body weight) agonists were administered 10 min prior to training, and EES was delivered throughout the session at S1 and L2 (cathodes vs. common ground at intracostal muscles). EES amplitude was selected to maximize locomotor performance. Drug dosage for rats with contusion SCI was adjusted over a few successive days in order to obtain the most stable walking conditions. Optimal body-weight support was defined as the minimum support level that they could sustain while maintaining appropriate extension and swing excursions without dragging (55%–65% of body weight). To evaluate the effect of body-weight support, we gradually decreased the level of support by fixed decrements of 5%.

Hindlimb kinematics was recorded using 12 infrared motion capture cameras (200 Hz; Vicon). Reflective markers were attached to anatomical landmarks of both hindlimbs (Figure 3B). Nexus (Vicon) was used to obtain 3D coordinates of the markers. EMG signals (12.207 kHz) were amplified and filtered online (10–5,000-Hz bandpass, AM-System). Vertical ground reaction forces were measured using a biomechanical force plate (2 kHz; HE6X6, AMTI) located below the treadmill belt. Video recordings (200 Hz) were obtained using two cameras (Basler Vision Technologies) oriented at 90° and 270° with respect to the direction of locomotion.

Processing of Kinematic, Ground Reaction Force, and Electromyographic Recordings

Data analysis and statistical procedures to process kinematic, ground reaction force and electromyographic have been described in detail previously (Courtine et al., 2009; van den Brand et al., 2012; Wenger et al., 2014).

Real-Time Monitoring and Stimulation Platform

The real-time monitoring and stimulation infrastructure was implemented within a multi-threaded C++ code (Visual Studio 2010, Microsoft) running on a quad-core Microsoft Windows 7 computer. Stimulation patterns were applied via an RZ5 processing unit (Tucker Davis Technologies) connected to an MS16 stimulus isolator (TDT). Raw 3D positions of markers were imported into the C++ environment (200 Hz) using a Datastream SDK software (Vicon). We used custom algorithms for online filtering (least mean squares adaptive filtering), interpolation (triangulation) and re-labeling of each marker (Wenger et al., 2014). Left and right foot strikes were automatically detected using online kinematic classification of limb endpoint trajectories. These gait events triggered controller calculations and model updates.

Controller Structure

The controller expanded the structure previously described in (Wenger et al., 2014) The continuous flow of bilateral kinematic information was discretized at bilateral foot strikes, which acted as sampling times $K = [k_i^R, k_i^L, k_{i+1}^R ...]$ and defined gait phases. Each separate hindlimb was then considered as a single-input single-output (SISO) system, independently of the other, and was controlled by separate controllers operating in parallel during one or the other gait phase. At each foot strike, the relevant controller evaluated the step height of the limb in swing (defined for the right phase as $h_i^R = max(h_t^{~R}), t \in [k_{i-1}^L, k_i^{~R}]$, and for the left phase as $h_i^L = max(h_t^L)$, $t \in [k_{i-1}^{~R}, k_i^{~L}]$), and corrected EES frequency to track a predefined reference height (r_{i+1}^R and r_{i+1}^L for the right and left phases, respectively; Figure S6). Corrections in EES frequency were obtained from a combination of feedback (PI control) and feedforward linear prediction (Wenger et al., 2014) but were only applied at the next iteration of the same phase.

Statistics

Experimental data and simulations were processed offline using MATLAB R2013b (MathWorks). All data are reported as mean values ± SD or SEM, as indicated. Normality of data was tested using a Kolmogorov-Smirnov test with 95% confidence interval (CI). A one-tailed t test with 95% CI was applied for comparison between conditions. Multi-group comparison was performed using a one-tailed ANOVA with 95% CI and Tukey-Kramer correction of the p value.

REFERENCES

Angeli, C.A., Edgerton, V.R., Gerasimenko, Y.P., and Harkema, S.J. (2014). Altering spinal cord excitability enables voluntary movements after chronic complete paralysis in humans. Brain *137*, 1394–1409.

Arber, S. (2012). Motor circuits in action: specification, connectivity, and function. Neuron *74*, 975–989.

Barbeau, H., McCrea, D.A., O'Donovan, M.J., Rossignol, S., Grill, W.M., and Lemay, M.A. (1999). Tapping into spinal circuits to restore motor function. Brain Res. Brain Res. Rev. *30*, 27–51.

Booth, V., Rinzel, J., and Kiehn, O. (1997). Compartmental model of vertebrate motoneurons for Ca2+-dependent spiking and plateau potentials under pharmacological treatment. J. Neurophysiol. *78*, 3371–3385.

Borton, D., Micera, S., Millán, Jdel.R., and Courtine, G. (2013). Personalized neuroprosthetics. Sci. Transl. Med. *5*, 210rv2.

Capaday, C. (2002). The special nature of human walking and its neural control. Trends Neurosci. *25*, 370–376.

Capogrosso, M., Wenger, N., Raspopovic, S., Musienko, P., Beauparlant, J., Bassi Luciani, L., Courtine, G., and Micera, S. (2013). A computational model

for epidural electrical stimulation of spinal sensorimotor circuits. J. Neurosci. *33*, 19326–19340.

Carhart, M.R., He, J., Herman, R., D'Luzansky, S., and Willis, W.T. (2004). Epidural spinal-cord stimulation facilitates recovery of functional walking following incomplete spinal-cord injury. IEEE Trans. Neural Syst. Rehabil. Eng. *12*, 32–42.

Cavagna, G.A., Willems, P.A., and Heglund, N.C. (2000). The role of gravity in human walking: pendular energy exchange, external work and optimal speed. J. Physiol. *528*, 657–668.

Clarac, F., Cattaert, D., and Le Ray, D. (2000). Central control components of a 'simple' stretch reflex. Trends Neurosci. *23*, 199–208.

Courtine, G., and Bloch, J. (2015). Defining ecological strategies in neuroprosthetics. Neuron *86*, 29–33.

Courtine, G., Gerasimenko, Y., van den Brand, R., Yew, A., Musienko, P., Zhong, H., Song, B., Ao, Y., Ichiyama, R.M., Lavrov, I., et al. (2009). Transformation of nonfunctional spinal circuits into functional states after the loss of brain input. Nat. Neurosci. *12*, 1333–1342.

Danner, S.M., Hofstoetter, U.S., Freundl, B., Binder, H., Mayr, W., Rattay, F., and Minassian, K. (2015). Human spinal locomotor control is based on flexibly organized burst generators. Brain *138*, 577–588.

Delp, S.L., Anderson, F.C., Arnold, A.S., Loan, P., Habib, A., John, C.T., Guendelman, E., and Thelen, D.G. (2007). OpenSim: open-source software to create and analyze dynamic simulations of movement. IEEE Trans. Biomed. Eng. *54*, 1940–1950.

Dietz, V., Wirz, M., Curt, A., and Colombo, G. (1998). Locomotor pattern in paraplegic patients: training effects and recovery of spinal cord function. Spinal Cord *36*, 380–390.

Edgerton, V.R., Courtine, G., Gerasimenko, Y.P., Lavrov, I., Ichiyama, R.M., Fong, A.J., Cai, L.L., Otoshi, C.K., Tillakaratne, N.J., Burdick, J.W., and Roy, R.R. (2008). Training locomotor networks. Brain Res. Brain Res. Rev. *57*, 241–254.

Ekeberg, O., and Pearson, K. (2005). Computer simulation of stepping in the hind legs of the cat: an examination of mechanisms regulating the stance-to-swing transition. J. Neurophysiol. *94*, 4256–4268.

Fleshman, J.W., Rudomin, P., and Burke, R.E. (1988). Supraspinal control of a short-latency cutaneous pathway to hindlimb motoneurons. Exp. Brain Res. *69*, 449–459.

Friedli, L., Rosenzweig, E.S., Barraud, Q., Schubert, M., Dominici, N., Awai, L., Nielson, J.L., Musienko, P., Nout-Lomas, Y., Zhong, H., et al. (2015). Pronounced species divergence in corticospinal tract reorganization and functional recovery after lateralized spinal cord injury favors primates. Sci. Transl. Med. *7*, 302ra134.

Gerasimenko, Y.P., Lavrov, I.A., Courtine, G., Ichiyama, R.M., Dy, C.J., Zhong, H., Roy, R.R., and Edgerton, V.R. (2006). Spinal cord reflexes induced by epidural spinal cord stimulation in normal awake rats. J. Neurosci. Methods *157*, 253–263.

Harrison, P.J., and Taylor, A. (1981). Individual excitatory post-synaptic potentials due to muscle spindle Ia afferents in cat triceps surae motoneurones. J. Physiol. *312*, 455–470.

Hines, M.L., and Carnevale, N.T. (1997). The NEURON simulation environment. Neural Comput. *9*, 1179–1209.

Hofstoetter, U.S., Danner, S.M., Freundl, B., Binder, H., Mayr, W., Rattay, F., and Minassian, K. (2015). Periodic modulation of repetitively elicited monosynaptic reflexes of the human lumbosacral spinal cord. J. Neurophysiol. *114*, 400–410.

Jankowska, E. (1992). Interneuronal relay in spinal pathways from proprioceptors. Prog. Neurobiol. *38*, 335–378.

Johnson, W.L., Jindrich, D.L., Roy, R.R., and Reggie Edgerton, V. (2008). A three-dimensional model of the rat hindlimb: musculoskeletal geometry and muscle moment arms. J. Biomech. *41*, 610–619.

Johnson, W.L., Jindrich, D.L., Hui, Z., Roy, R.R., and Edgerton, V.R. (2011). Application of a rat hindlimb model: a prediction of force spaces reachable

through stimulation of nerve fascicles. Biomedical Engineering. IEEE Trans. Biomed. Eng. *58*, 3328–3338.

Jones, K.E., and Bawa, P. (1997). Computer simulation of the responses of human motoneurons to composite 1A EPSPS: effects of background firing rate. J. Neurophysiol. *77*, 405–420.

Kiehn, O. (2006). Locomotor circuits in the mammalian spinal cord. Annu. Rev. Neurosci. *29*, 279–306.

Lacquaniti, F., Ivanenko, Y.P., and Zago, M. (2012). Development of human locomotion. Curr. Opin. Neurobiol. *22*, 822–828.

Levine, A.J., Hinckley, C.A., Hilde, K.L., Driscoll, S.P., Poon, T.H., Montgomery, J.M., and Pfaff, S.L. (2014). Identification of a cellular node for motor control pathways. Nat. Neurosci. *17*, 586–593.

McIntyre, C.C., and Foutz, T.J. (2013). Computational modeling of deep brain stimulation. In Handbook of Clinical Neurology, P.J. Vinken and G.W. Bruyn, eds. (Elsevier), pp. 55–61.

McIntyre, C.C., and Grill, W.M. (2002). Extracellular stimulation of central neurons: influence of stimulus waveform and frequency on neuronal output. J. Neurophysiol. *88*, 1592–1604.

McIntyre, C.C., Richardson, A.G., and Grill, W.M. (2002). Modeling the excitability of mammalian nerve fibers: influence of afterpotentials on the recovery cycle. J. Neurophysiol. *87*, 995–1006.

Minev, I.R., Musienko, P., Hirsch, A., Barraud, Q., Wenger, N., Moraud, E.M., Gandar, J., Capogrosso, M., Milekovic, T., Asboth, L., et al. (2015). Biomaterials: electronic dura mater for long-term multimodal neural interfaces. Science *347*, 159–163.

Munson, J.B., Fleshman, J.W., and Sypert, G.W. (1980). Properties of single-fiber spindle group II EPSPs in triceps surae motoneurons. J. Neurophysiol. *44*, 713–725.

National Institutes of Health (2015). Framework for a research study on epidural spinal stimulation to improve bladder, bowel, and sexual function in individuals with spinal cord injuries. http://www.nibib.nih.gov/2015-nibib-consortium-report.

Orlovsky, G.N., Deliagina, T.G., and Grinllner, S. (1999). Neuronal Control of Locomotion: From Mollusc to Man (Oxford University Press).

Pearson, K.G. (1993). Common principles of motor control in vertebrates and invertebrates. Annu. Rev. Neurosci. *16*, 265–297.

Pierrot-Deseilligny, E. (1989). Peripheral and descending control of neurones mediating non-monosynaptic Ia excitation to motoneurones: a presumed propriospinal system in man. Prog. Brain Res. *80*, 305–314, discussion 295–297.

Pratt, C.A., and Jordan, L.M. (1987). Ia inhibitory interneurons and Renshaw cells as contributors to the spinal mechanisms of fictive locomotion. J. Neurophysiol. *57*, 56–71.

Prochazka, A., and Gorassini, M. (1998a). Ensemble firing of muscle afferents recorded during normal locomotion in cats. J. Physiol. *507*, 293–304.

Prochazka, A., and Gorassini, M. (1998b). Models of ensemble firing of muscle spindle afferents recorded during normal locomotion in cats. J. Physiol. *507*, 277–291.

Quevedo, J., Fedirchuk, B., Gosgnach, S., and McCrea, D.A. (2000). Group I disynaptic excitation of cat hindlimb flexor and bifunctional motoneurones during fictive locomotion. J. Physiol. *525*, 549–564.

Rattay, F., Minassian, K., and Dimitrijevic, M.R. (2000). Epidural electrical stimulation of posterior structures of the human lumbosacral cord: 2. quantitative analysis by computer modeling. Spinal Cord *38*, 473–489.

Rossignol, S., Dubuc, R., and Gossard, J.P. (2006). Dynamic sensorimotor interactions in locomotion. Physiol. Rev. *86*, 89–154.

Rybak, I.A., Stecina, K., Shevtsova, N.A., and McCrea, D.A. (2006). Modelling spinal circuitry involved in locomotor pattern generation: insights from the effects of afferent stimulation. J. Physiol. *577*, 641–658.

Sayenko, D.G., Angeli, C., Harkema, S.J., Edgerton, V.R., and Gerasimenko, Y.P. (2014). Neuromodulation of evoked muscle potentials induced by epidural spinal-cord stimulation in paralyzed individuals. J. Neurophysiol. *111*, 1088–1099.

Scott, J.G., and Mendell, L.M. (1976). Individual EPSPs produced by single triceps surae Ia afferent fibers in homonymous and heteronymous motoneurons. J. Neurophysiol. *39*, 679–692.

Segev, I., Fleshman, J.W., Jr., and Burke, R.E. (1990). Computer simulation of group Ia EPSPs using morphologically realistic models of cat alpha-motoneurons. J. Neurophysiol. *64*, 648–660.

Sherrington, C.S. (1910). Flexion-reflex of the limb, crossed extension-reflex, and reflex stepping and standing. J. Physiol. *40*, 28–121.

Song, S., and Geyer, H. (2015). A neural circuitry that emphasizes spinal feedback generates diverse behaviours of human locomotion. J. Physiol. *593*, 3493–3511.

Stienen, A.H., Schouten, A.C., Schuurmans, J., and van der Helm, F.C. (2007). Analysis of reflex modulation with a biologically realistic neural network. J. Comput. Neurosci. *23*, 333–348.

Talpalar, A.E., Endo, T., Löw, P., Borgius, L., Hägglund, M., Dougherty, K.J., Ryge, J., Hnasko, T.S., and Kiehn, O. (2011). Identification of minimal neuronal networks involved in flexor-extensor alternation in the mammalian spinal cord. Neuron *71*, 1071–1084.

Tripodi, M., Stepien, A.E., and Arber, S. (2011). Motor antagonism exposed by spatial segregation and timing of neurogenesis. Nature *479*, 61–66.

van den Brand, R., Heutschi, J., Barraud, Q., DiGiovanna, J., Bartholdi, K., Huerlimann, M., Friedli, L., Vollenweider, I., Moraud, E.M., Duis, S., et al. (2012). Restoring voluntary control of locomotion after paralyzing spinal cord injury. Science *336*, 1182–1185.

Wenger, N., Moraud, E.M., Raspopovic, S., Bonizzato, M., DiGiovanna, J., Musienko, P., Morari, M., Micera, S., and Courtine, G. (2014). Closed-loop neuromodulation of spinal sensorimotor circuits controls refined locomotion after complete spinal cord injury. Sci. Transl. Med. *6*, 255ra133.

Zhang, T.C., Janik, J.J., and Grill, W.M. (2014). Mechanisms and models of spinal cord stimulation for the treatment of neuropathic pain. Brain Res. *1569*, 19–31.